International Journal of Naval Architecture and Ocean Engineering 15 (2023) 100492

Contents lists available at ScienceDirect

International Journal of Naval Architecture and Ocean Engineering

journal homepage: www.journals.elsevier.com/international-journal-of-naval-architecture-and-ocean-engineering/

Experimental study on the cavitation flow and motion characteristics of the vehicle launched underwater

Yao Shi [a,b,*], Jiewen Lu [a,b], Shan Gao [a,b], Guang Pan [a,b], Jinyi Ren [a,b]

[a] School of Marine Science and Technology, Northwestern Polytechnical University, Xi'an, 710072, China
[b] Key Laboratory for Unmanned Vehicle, Northwestern Polytechnical University, Xi'an, 710072, China

ARTICLE INFO

Keywords:
Vehicle
Underwater launch
Cavitation flow
Water-exiting
Motion characteristics

ABSTRACT

In this paper, an experimental system was independently designed to investigate the cavitation flow mechanism and motion characteristic of the vehicle launched underwater. Conducted experiments based on high-speed photography, and the influence of cavity morphological evolution and kinematic characteristics with the different launch and transverse velocities were analyzed. The results show that cavity shedding phenomenon occurs on different scales. Subsequently, a wide range of pressure impulse on the surface of the vehicle is caused by the collapse of large-scale cavity groups, resulting in an obvious sputtering phenomenon on its surface during the water-exit stage. The more the launch speed increases, the longer the initial cavity length is. Moreover, the moment of completely shedding the cavity delays during the water exit process; Furthermore, with the increase of transverse speed, the attitude angle generally shows an increasing trend, but its growth rate slowed down during the large-scale shedding stage of the cavity.

1. Introduction

Local low-pressure areas are formed on the surface of the vehicle, due to the bypassing effect of water. Subsequently, vaporization occurs, resulting in cavitation phenomena when the pressure is less than the saturation vapor pressure of the underwater launched vehicle. The generation, shedding, and collapse of cavities are crucial physical phenomena, which have an essential influence on the motion and motion parameters (Blake and Gibson, 1987; Wang et al., 2015; Gao et al., 2022a, 2022b; Callenaere et al., 2001; Leroux et al., 2004; Franc and Michel, 2006).

Scholars have undertaken substantial research on pumps (Xu et al., 2021; Li et al., 2019; Ramirez et al., 2020), nozzles (Marian et al., 2020; Wang et al., 2017), hydrofoils (Yin et al., 2022; Pant and Frankel, 2021; Ausoni et al., 2007; Sun et al., 2021a), propellers (Zhao et al., 2020; Huang et al., 2020; Hu et al., 2021), and axisymmetric cylinders (Chen et al., 2021; Louf et al., 2018; Tan et al., 2022; Boštjan et al., 2010)for cavitation phenomena, including numerical simulations and experiments. The two most important common conclusions regarding cavitation: the cavitation development and shedding mechanism, involve the re-entry jet interaction mechanism in classical multiphase flow; The high-speed jets produced by the collapse of the complicated cavity directly to the structure and may damage it. Sun et al. (2021b) studied the cavitation evolution and pressure pulsation characteristics. The results show that the evolution of cloud cavitation can be mainly divided into three stages: (I) the growth process of the attached cavity, (II) the shedding process of the attached cavity, and (III) the collapse of detached cavities. The evolution of the attached cavity and the collapse of the large-scale shedding cavity will cause strong pressure pulsations. It is found that the cavitation number plays an important role in cavitation evolution and pressure pulsation. Lu et al. (2022a) establish an independent bubble evolution model to predict the internal cavity pressure based on the assumption of spherical expansion; they also separately construct a shoulder cavity evolution model that treats the cavity as a slender body. Reached the effects of cavity pressure oscillations and the nose shape and vehicle velocity on the cavity's behavior are studied.

To lessen the collapse stress induced by unstable cavitation, some researchers recommended the method of ventilation, which included numerical simulation and experimental study (Kawakami and Arndt, 2010; Shao et al., 2018; Jin et al., 2011; Gao et al., 2021; ShiRen et al., 2021; Zhang et al., 2016). Wang et al. (Yu et al., 2015) studied the physical process of drag reduction in axisymmetric bodies by injecting

Peer review under responsibility of Society of Naval Architects of Korea.
* Corresponding author. School of Marine Science and Technology, Northwestern Polytechnical University, Xi'an, 710072, China.
E-mail address: shiyao@nwpu.edu.cn (Y. Shi).

https://doi.org/10.1016/j.ijnaoe.2022.100492
Received 16 September 2022; Received in revised form 31 October 2022; Accepted 14 November 2022
Available online 21 November 2022
2092-6782/© 2022 Published by Society of Naval Architects of Korea. This is an open access article under the CC BY-NC-ND license (http://creativecommons.org/licenses/by-nc-nd/4.0/).

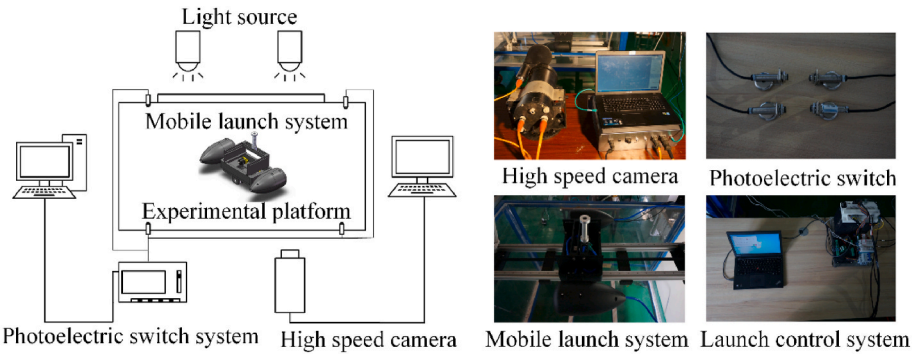


Fig. 1. The overall schematic diagram of the experimental setup and some physical pictures.

air, a comparison between numerical and experimental air layer length shows a good correlation. Results indicate that the air layer has a good effect on drag reduction. And Sun et al. (2022) studied the front propeller on the cavity ship, which will promote the development of ventilated cavity downstream. The result shows that the submerged body interferes with the characteristics of the propeller blade tip vortex downstream and affects the hydrodynamic performance of the structure, including thrust and drag. Ventilation over the surface of the submerged body results in lower propeller efficiency and less drag. Meanwhile, ventilated cavity presents an obvious effect on the velocity field and vorticity field around the submerged body.

The study of cavitation phenomena is extremely challenging due to the complicated environment of the underwater launched vehicles. Wang et al. studied the effect of free surface on unsteady cloud cavitation on high-speed surface vehicles and concluded that the evolution of the cavity on the upper side of the vehicle is significantly different from the evolution of the cavity on the lower side of the vehicle. There is a clear difference compared to the underside under the free surface effect. Second, the effects of free surfaces are investigated by analyzing changes in constraints. Finally, the wave rise heights with and without cavitation are compared (Wang et al., 2016); In addition, a new internal collapse phenomenon that advances from the tail to the head of the axisymmetric vehicle has been observed in an underwater launched experiment: it differs from the usual collapse phenomena and is rarely observed in water tunnel tests. During this process, cavities shrink upstream quickly, producing high impact pressure, and fast re-entry jets form, inducing strong instabilities. Analysis indicates this phenomenon is relative to rapid changes in vehicle speed and cavitation number (Wang et al., 2016). Quan et al. (2008) conducted experimental and computational studies on the process of cavitation collapse, found some laws of cavitation collapse, and discussed the factors and mechanisms affecting cavitation collapse. It is concluded that cavitation occurs on the surface of the vehicle when it moves at high speed underwater. In the process of water exit, the collapse of cavitation occurs, which has an important impact on the surface force and mechanical environment of the vehicle. Lu et al. (2022b) conducted an experimental study and found that in the successive underwater launch of two vehicles, wake vortices shed from the leading vehicle have significant effects on the subsequent vehicle's hydrodynamic forces, attitude, and trajectory.

In summary, the majority of research has focused on cavitation stability and vehicle wake, while there have been relatively few experimental studies on the morphological evolution of the cavity and motion characteristics. As a result, based on the self-designed underwater launched platform, this paper investigates the evolution mechanism of the cavitation and the motion characteristics in the scaled-down model with the different launch speeds and transverse velocities.

2. Experimental setup

In this paper, established an experimental platform that can conduct the underwater vertically launched vehicle, and the schematic diagram is illustrated in Fig. 1. It mainly consists of a small transparent water tank, vehicle launch device, control device of transverse velocity, lighting system, data collection system, and the launch experiment with different launch velocities are accomplished by adjusting the size of air pressure in the storage cylinder. The transparent water tank size is 1.84m × 1.2m × 1.22 m, the control device of transverse velocity is to simulate the effect of transverse flow in the actual underwater launched vehicle, the effective distance of the horizontal movement of the device is 0.8 m, and the maximum transverse velocity that the device can achieve is 3 m/s. To capture the motion posture and cavity morphology of the vehicle clearly after launch, two 500 W illumination lamps are arranged at the back of the tank for the experimental light source. The high-speed camera used in the experiment has a resolution of 576 × 1080, a frame rate of 3000 fps, and an exposure time of 200 μs.

The vehicle model used in the experiment is a scaled-down with the type of a hemispherical head, 20 mm in diameter, and a slenderness ratio of 6, constructed of 2A12 aluminum alloy, and the model is designed in portions to lower the quality of the model. The interior hollow, 3 mm wall thickness, and threaded and radially sealed segments assure no water seepage after each experiment. All of the surfaces are anodized in natural color, and there are no obvious scratches or flaws.

Table 1
Summary of symbols and parameters.

Parameter	Symbol	value
Length of the vehicle (mm)	L	120
Radius of the vehicle (mm)	D	20
Quality of the vehicle (g)	m	60.4
Water density (kg/m^3)	ρ_w	998
Launch depth (mm)	H	465
Launch velocity (m/s)	v_p	14.5,17.2,20.0,23.5
Transverse velocity (m/s)	v_b	0.5,1.0,1.5
Gravitational acceleration (m/s^2)	g	9.8
Cavitation number	$\sigma = \frac{P_0 - P_{va} + \rho_w g H}{\frac{1}{2} v_p^2 \rho_w}$	/
Dimensionless time	$\bar{t} = \frac{t v_p}{D}$	/
Dimensionless horizontal displacement	$\bar{x} = \frac{x}{D}$	/
Dimensionless vertical displacement	$\bar{z} = \frac{z}{D}$	/
Dimensionless angle	$\bar{\theta} = \frac{\theta}{\theta_0}$	/

3. Parameters

To make this paper more readable, all symbols presented in this paper are listed in Table 1.

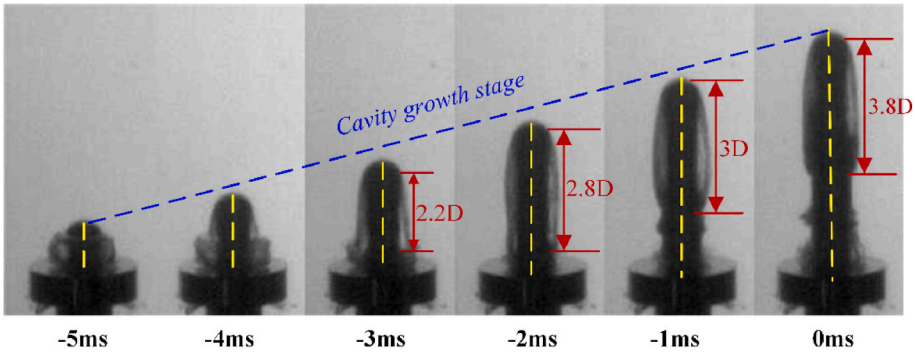


Fig. 2. Cavitation phenomenon during the tube-exit stage.

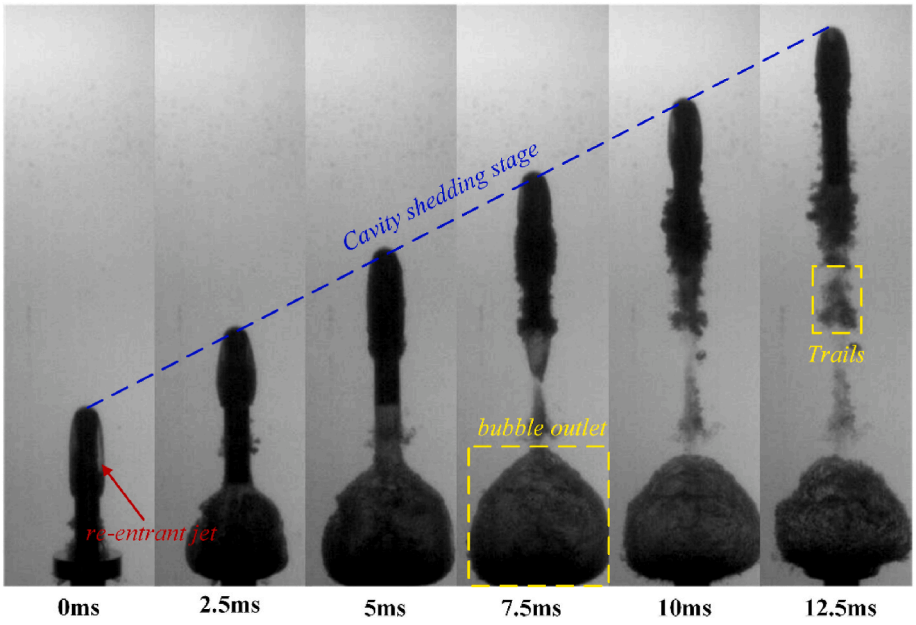


Fig. 3. Cavitation phenomenon during the traveling stage.

4. Results and discussion

4.1. Mechanism of cavitation evolution

The experimental images of the tube-exit stage, the water-traveling stage, and the water-exit stage are shown in Fig. 2, Fig. 3, and Fig. 4 (23.5 m/s, depth of 0.465 m), respectively. For the subsequent analysis, the moment of the vehicle tail just leaving the tube mouth is defined as the zero moment (t = 0 ms).

As shown in Fig. 2, the vehicle from a standstill to the beginning of the movement, the tube-outlet is squeezed by the vehicle making the film on the tube mouth expand outward, then, the film is broken when it can withstand the maximum tension which is less than the pressure of the tube mouth gas. The vehicle passes through the tube outlet with the process of continuous acceleration and forms a low-pressure region in the shoulder, thus generating an initial shoulder cavity (t = −5 ms). The cavity keeps elongating and increasing in volume with the upward movement of the vehicle (t = −4 ms). When the cavity length reaches a certain value, a significant contraction phenomenon occurs in the tail (t = −2 ms). The shoulder cavity is separated from the tube outlet (i.e., closure occurs at the tail of the cavity, t = -1 ms) until the shoulder cavity shrinks to the diameter equal to the vehicle diameter. The trailing closure of the cavity then forms a flow standing point, which drives the re-entry jet to be generated and causes the re-entry jet to move toward the interior of the cavity. The fracture and collapse of the cavity tail begin to occur (t = 0 ms) under the combined effect of the re-entry jet and the contraction of the cavity tail.

As seen in Fig. 3, the shoulder cavity occurs fracture phenomenon under the impact of the re-entry jet (t = 2.5 ms) after leaving the mouth of the tube. The vehicle speed keeps decreasing in the procedure of upward movement, and thus the pressure keeps rising in its shoulder region. Next, the re-entry jet intersects with the external fluid, thereby shearing the cavity substantially and making the majority of the cavity detached and separated from the vehicle surface (t = 7.5 ms) when the re-entry jet moves to the front of the cavity. At this time, the shoulder still has a partially attached cavity remaining. Subsequently, the vehicle moves upward and the cavity is continuously shed downstream along its surface (t = 10–12.5 ms).

Fig. 4 depicts the stage of the collapsed cavity. The medium around the cavity changes from water to air (t = 15.5 ms), which makes the cavity disappear from its condition for existence in the process of crossing the free liquid surface. Thereafter, the cavities attached to the vehicle surface slip downward (t = 17 ms) and the remained cavities move upward. This cavity was accelerated to move radially inward, impacting the vehicle surface, and bounced back to move radially outward with the pressure difference between the internal and external. Thereby, causing the cavity to collapse and forming a distinct splash phenomenon near the vehicle surface (t = 20 ms).

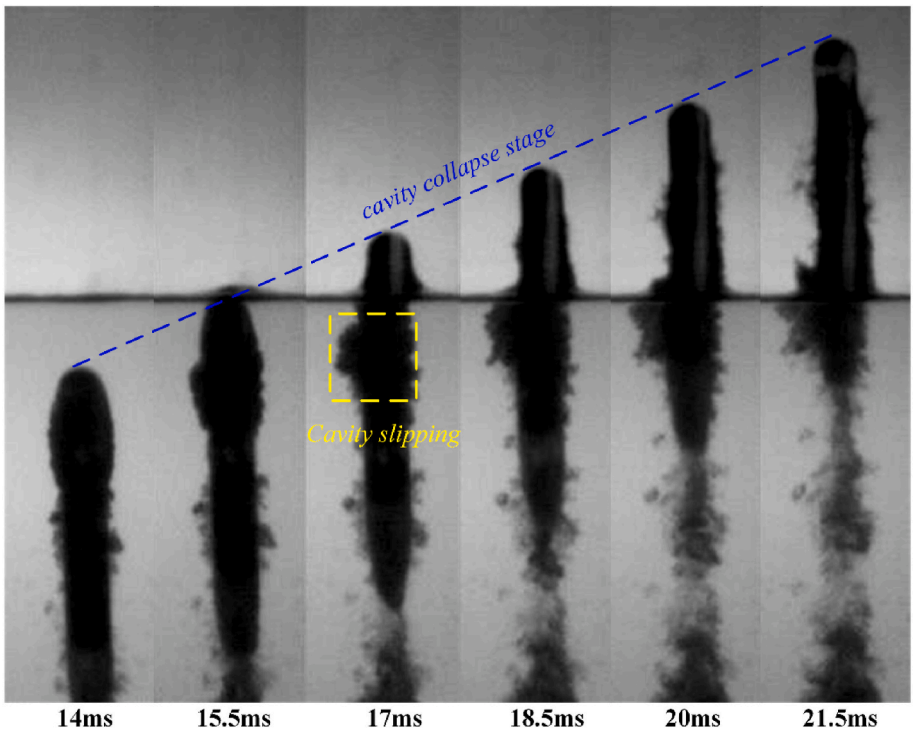


Fig. 4. Cavitation phenomenon during the water-exit stage.

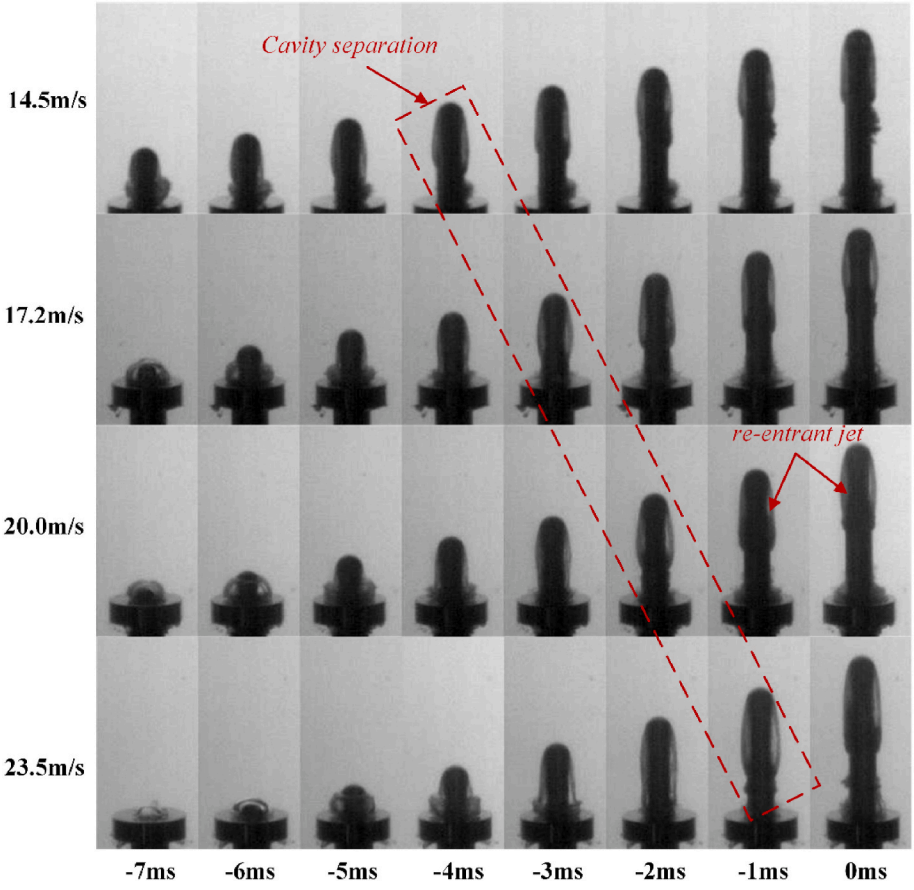


Fig. 5. Comparison of cavitation during the tube-exit stage.

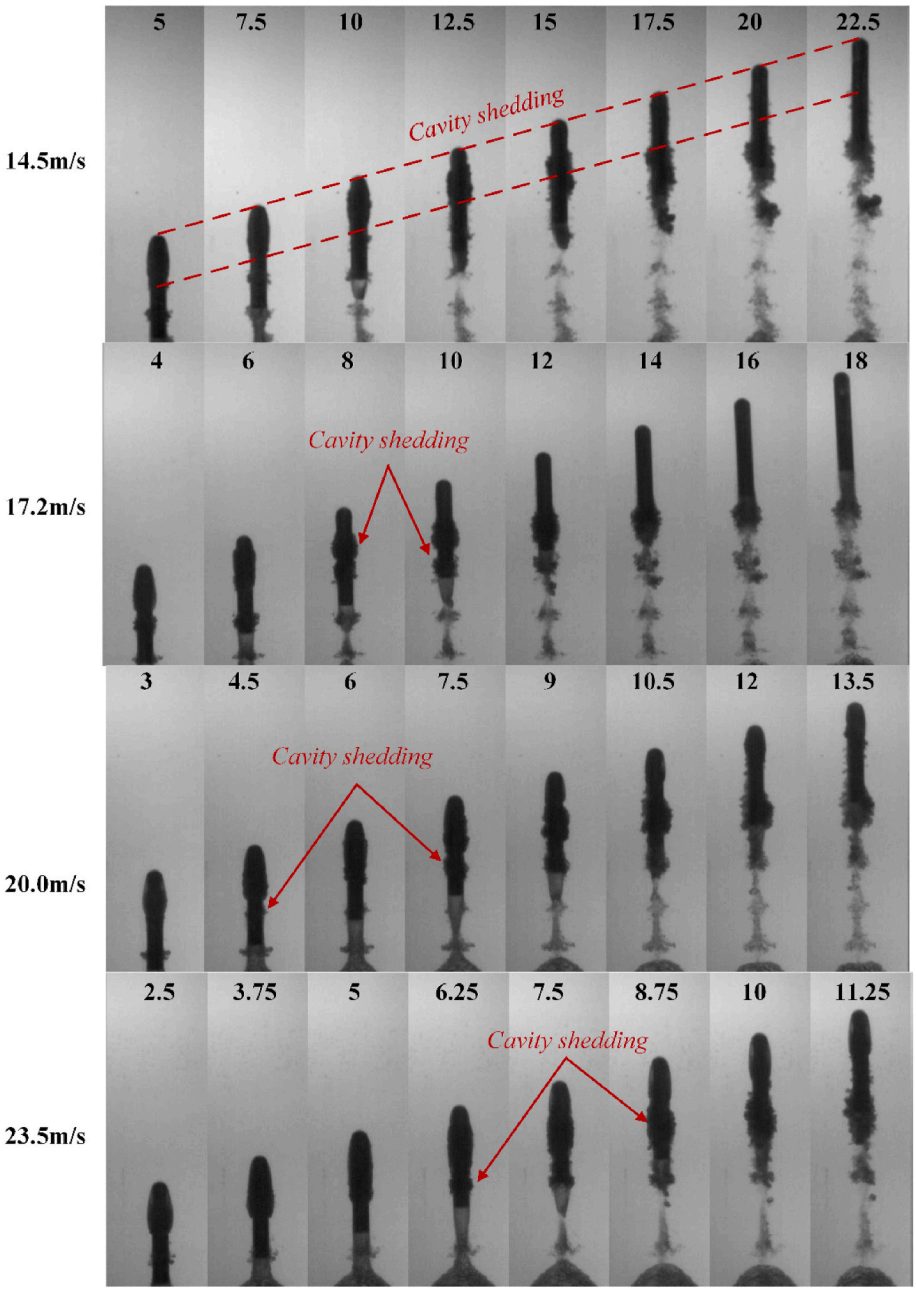


Fig. 6. Comparison of cavitation during the traveling stage.

4.2. Effect of flow field evolution characteristics with different launch speeds

4.2.1. Effect of cavity evolution with different launch speeds

Fig. 5 depicts the experimental images of the tube-exit stage launched underwater in a still water environment with launch speeds (14.5 m/s, 17.2 m/s, 20.0 m/s, and 23.5 m/s).

As the speed increases, the separation of the cavity from the tube outlet occurs later and the length of the cavity is longer. At the same time, the lower pressure region in the shoulder is increasing. This is primarily due to increased velocity, which increases the amount of gas flowing from the tube outlet to the cavity, resulting in the time-delayed of cavity separation and a larger axial development scale.

Fig. 6 shows experimental images with four different conditions (14.5 m/s, 17.2 m/s, 20.0 m/s, and 23.5 m/s) in the water-traveling stage to examine the evolution of the cavity flow characteristics. Since the velocities differ, the specific moments at which the experimental images for each working condition are shown in the figure. The behavior of cavity shedding is similar for different conditions. However, the frequency and scale of cavity shedding differ.

The period of cavity shedding and the scale of the remaining attached cavities both have significant differences with different velocities. It has been discovered that the period of cavity shedding shortens as velocity increases. Following the large-scale shedding of cavities, the attached cavities were virtually completely shed with the velocity of 14.5 m/s and 17.2 m/s.

However, after the large-scale cavity shedding (20.0 m/s condition, t = 10.5 ms; 23.5 m/s cases, t = 7.5 ms), new attached cavities grew on the shoulder, and the length of the cavities was significantly shorter than that of the previously attached cavities with the velocity of 20.0 m/s and 23.5 m/s.

The scale of attached cavities varies depending on the velocity, which also has an impact on the cavity collapse process during the water exit period. Fig. 7 shows experimental images of the water exit phase to

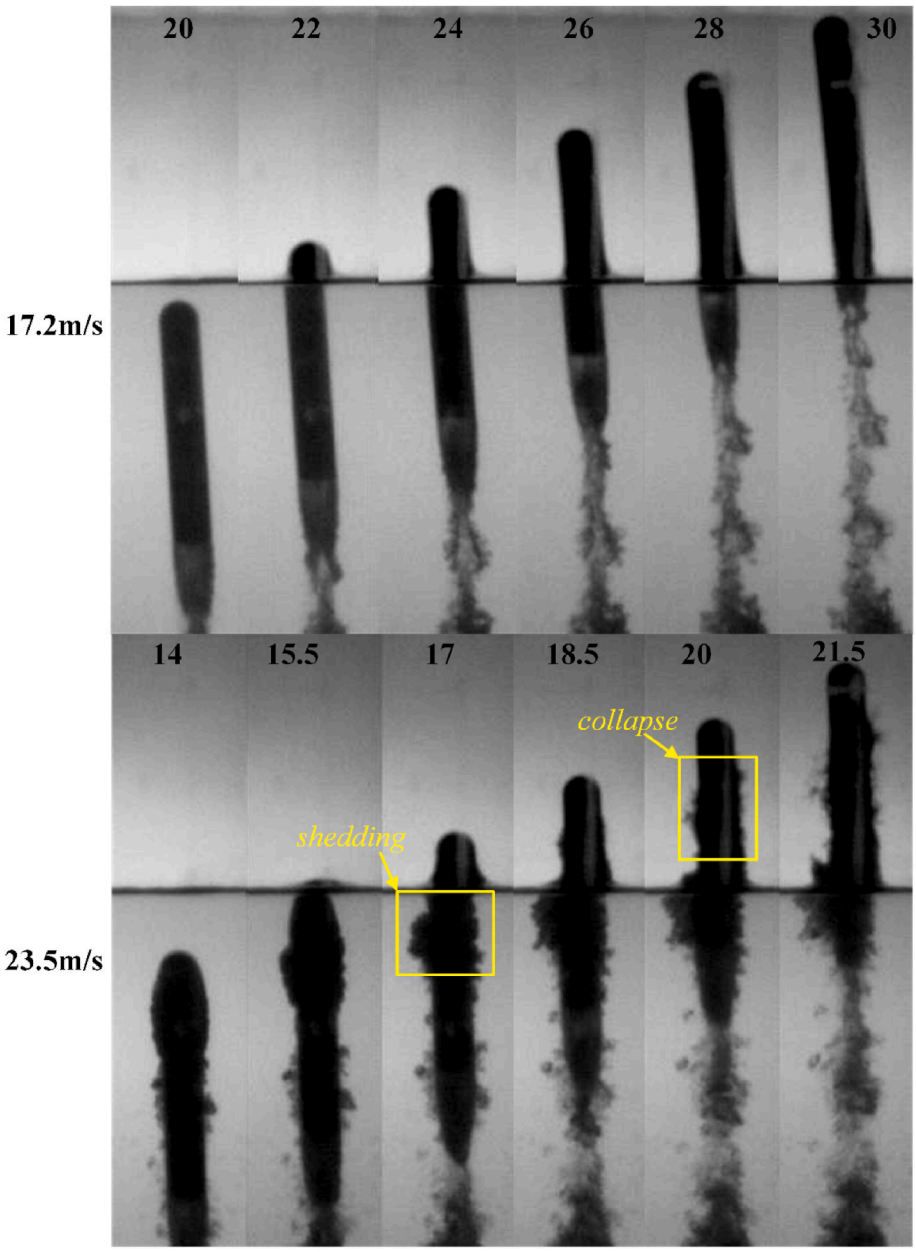


Fig. 7. Comparison of cavitation during the water-exit stage.

examine the evolution of flow characteristics with different velocities, where the shoulder at 17.2 m/s has no cavities out of the water and the shoulder at 23.5 m/s has attached cavities across the free liquid surface. As a result, there are clear differences in the evolution of the attached water layer on the vehicle surface in these two operating conditions.

When the head is near the free liquid surface, the vehicle contacted part converts from aqueous to the gas medium. As the vehicle moves upward, a thin layer of water attaches to the surface of the head effect of surface tension, and the attached layer of water slides downward along its surface by gravity in the absence of the shoulder attachment cavity out of the water. As the vehicle tail with the tail cavity, part of the liquid is also brought out together and meets with the surface of the water layer sliding down in the process of the tail leaving the water. After the tail exits (t = 30 ms), the tail cavity collapses as a result of the pressure differential between the interior and exterior of the wake cavity.

The thin layer of water outside the cavity comes into contact with the external atmosphere as the shoulder crosses the water surface, and the pressure inside the cavity is much lower than the atmospheric pressure. As a result of the pressure difference between the inside and outside, the water layer was accelerated radially inward, lashing the wall and being bounced back to radially outward motion, resulting in the collapse of the cavity. Eventually, a noticeable splash phenomenon was formed near the vehicle surface (t = 20 ms).

Fig. 8 shows the definitions of the cavity length and thickness to analyze the influence law of the morphological evolution characteristics of the cavity with different speeds. Fig. 9 depicts the variation in cavity length and maximum thickness over time in the stage of tube exit.

The speed is increasing, and the cavity is lengthening as it exits the tube, so the cavity length as a whole is rising. Since the gas inside the cavity which is constantly expanding and contracting, its thickness fluctuates in a manner that is consistent with this. The figure shows that as speed increases, the length of the shoulder cavity increases, and the thickness of the cavity increases in a corresponding trend between-2ms~0 ms and 2 ms~5 ms.

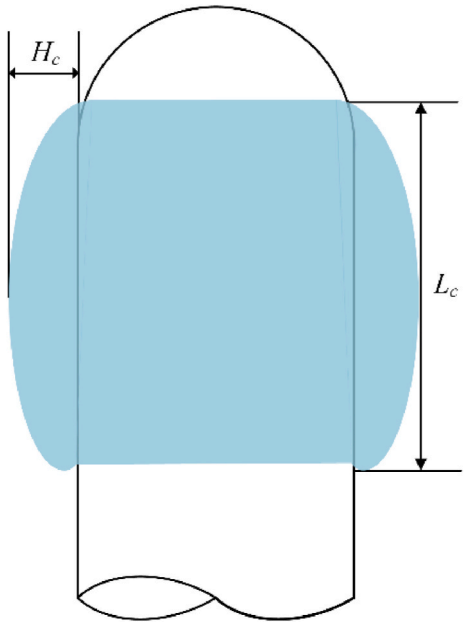


Fig. 8. Defines the length and thickness of the shoulder cavity.

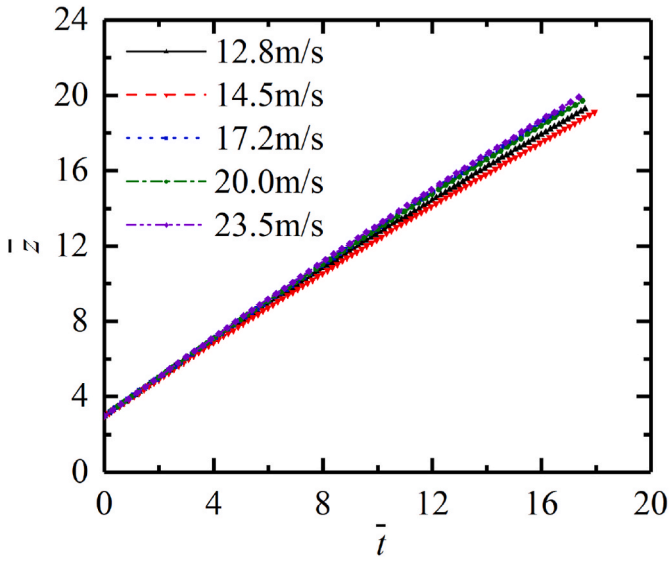


Fig. 10. Comparison of vertical displacement.

4.2.2. Effect of motion characteristics with different launch velocities

Fig. 10 depicts a comparison graph of the dimensionless vertical displacement variation with different velocities in the water traveling stage. It is discovered that the variation of the dimensionless displacement of the vehicle is virtually identical, with modest differences between them. This is primarily caused by the fact that the differential pressure resistance dominates the flow resistance; However, the proportion of frictional resistance is quite limited. In other words, the effect of speed on the variation of the vertical displacement is quite slight in this stage.

The variation of vehicle cavitation number is primarily influenced by speed and depth, and Fig. 11 depicts the variation curves of cavitation number with dimensionless time with different speeds. The velocity is still rising in the initial moment of the tube mouth, so the cavitation number is decreasing, as determined by the cavitation number curve with 12.8 m/s velocity. Following that, the vehicle decelerates continuously, and the cavitation number increases attributable to flow resistance, corresponding to an increase in cavity shedding size and a shortening of length. The upward motion is accompanied by a constant loss of depth and velocity. However, depth is positively related to cavitation number, while velocity is negatively related to cavitation number. Thus, based on the overall increasing cavitation number in

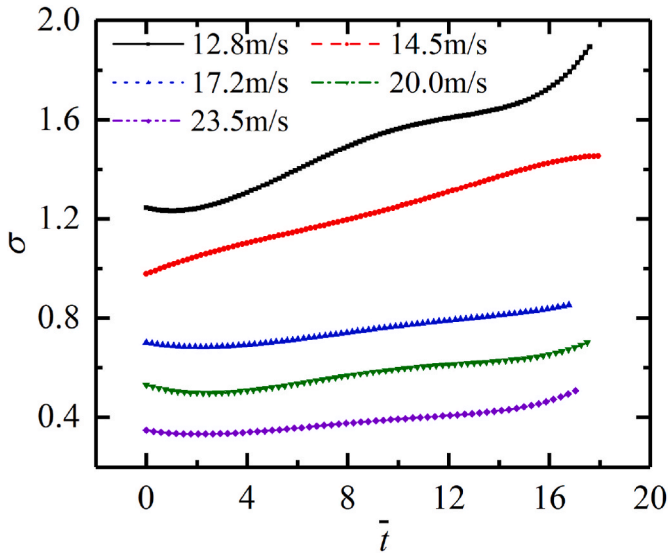
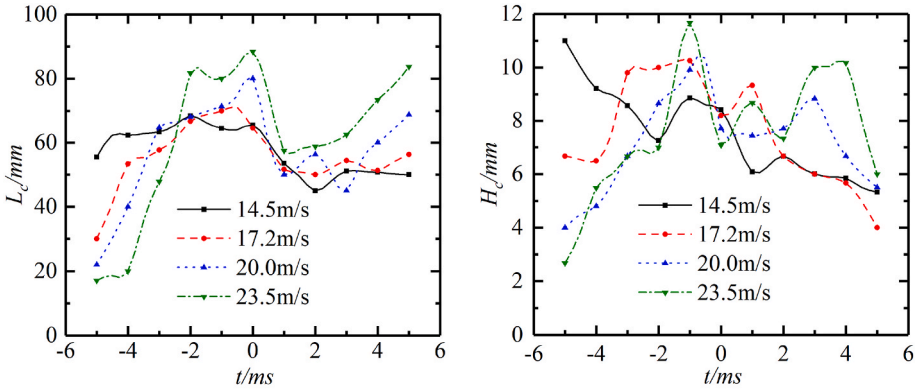


Fig. 11. Comparison of cavitation number.



(a) Variation in cavity length (b) Variation in cavity thickness

Fig. 9. Graph of cavity dimensions over time.

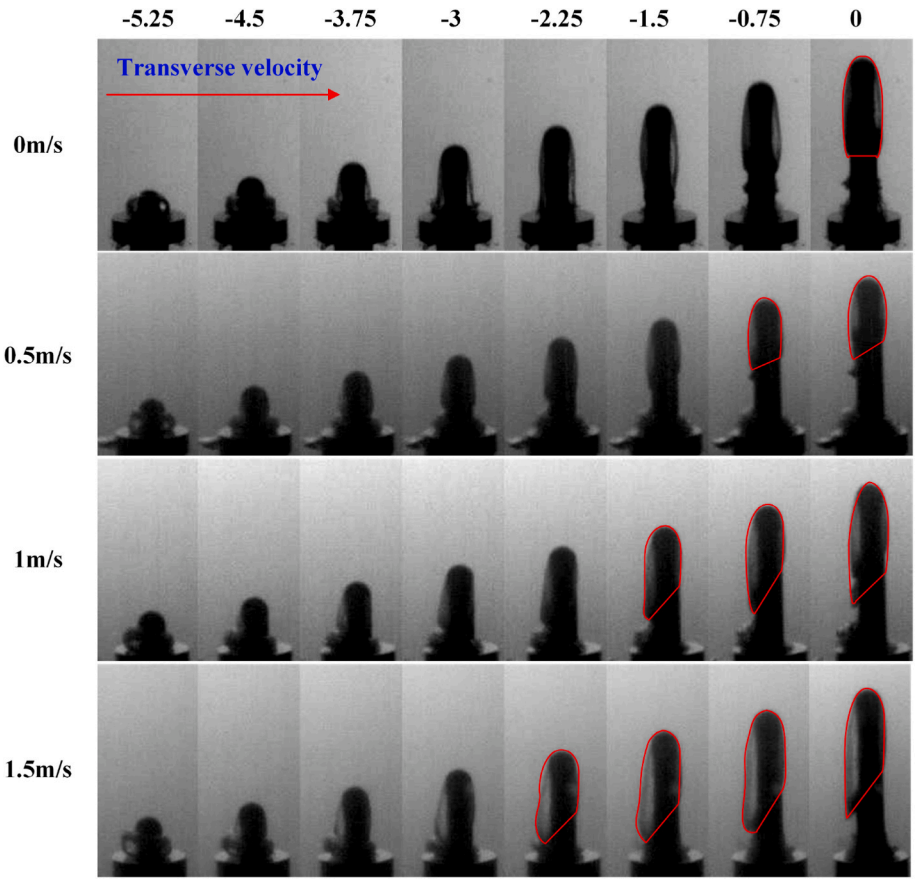


Fig. 12. Comparison of cavitation during the tube-exit stage.

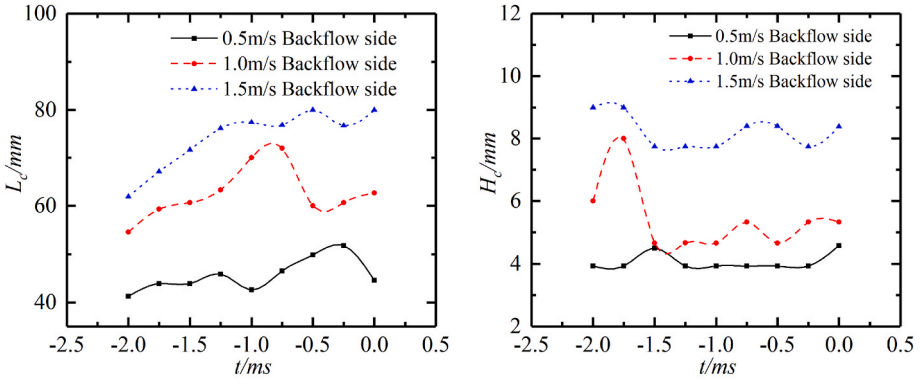
Fig. 11, it is clear that the effect of speed on the cavity evolution in this experiment is far greater than the effect of depth.

4.3. Effect of the flow field characteristics with different transverse velocities

4.3.1. Effect of the cavity evolution with different transverse velocities

Fig. 12 depicts the experimental images with different transverse velocities (0.0 m/s, 0.5 m/s, 1.0 m/s, and 1.5 m/s; launched speed of 23.5 m/s; depth of 0.465 m) in the tube-exit stage. The cavity contour line, shown in red in the figure, is used to indicate the asymmetry of the shoulder cavity.

Because the transverse velocity direction is from left to right, the images taken experimentally define the right side of the vehicle as the on-flow side and the left side as the back-flow side. The evolution of the cavity in the tube-exit stage is illustrated by the experimental working condition with 1.5 m/s transverse velocity. During the expansion phase of the tube outlet, the air mass expands unevenly, resulting in a slightly larger expansion on the back-flow side than on the on-flow side ($t = -5.25$ ms). Following that, the vehicle head passes through the tube outlet and creates a flow separation at the shoulder, resulting in the formation of an initial cavity ($t = -4.5$ ms). After that, the cavity keeps growing and lengthening while the tube outlet keeps shrinking and collapsing, with the back-flow side of the cavity's expansion scale being noticeably larger than the on-flow side ($t = -3$ ms). The cavity separates from the tube outlet when the length of the cavity on the back-flow side reaches a certain value ($t = -0.75$ ms). The attached cavity is continuously stretched as the vehicle accelerates upward, resulting in a



(a) Variation in cavity length (b) Variation in cavity thickness

Fig. 13. Graph of cavity dimensions over time.

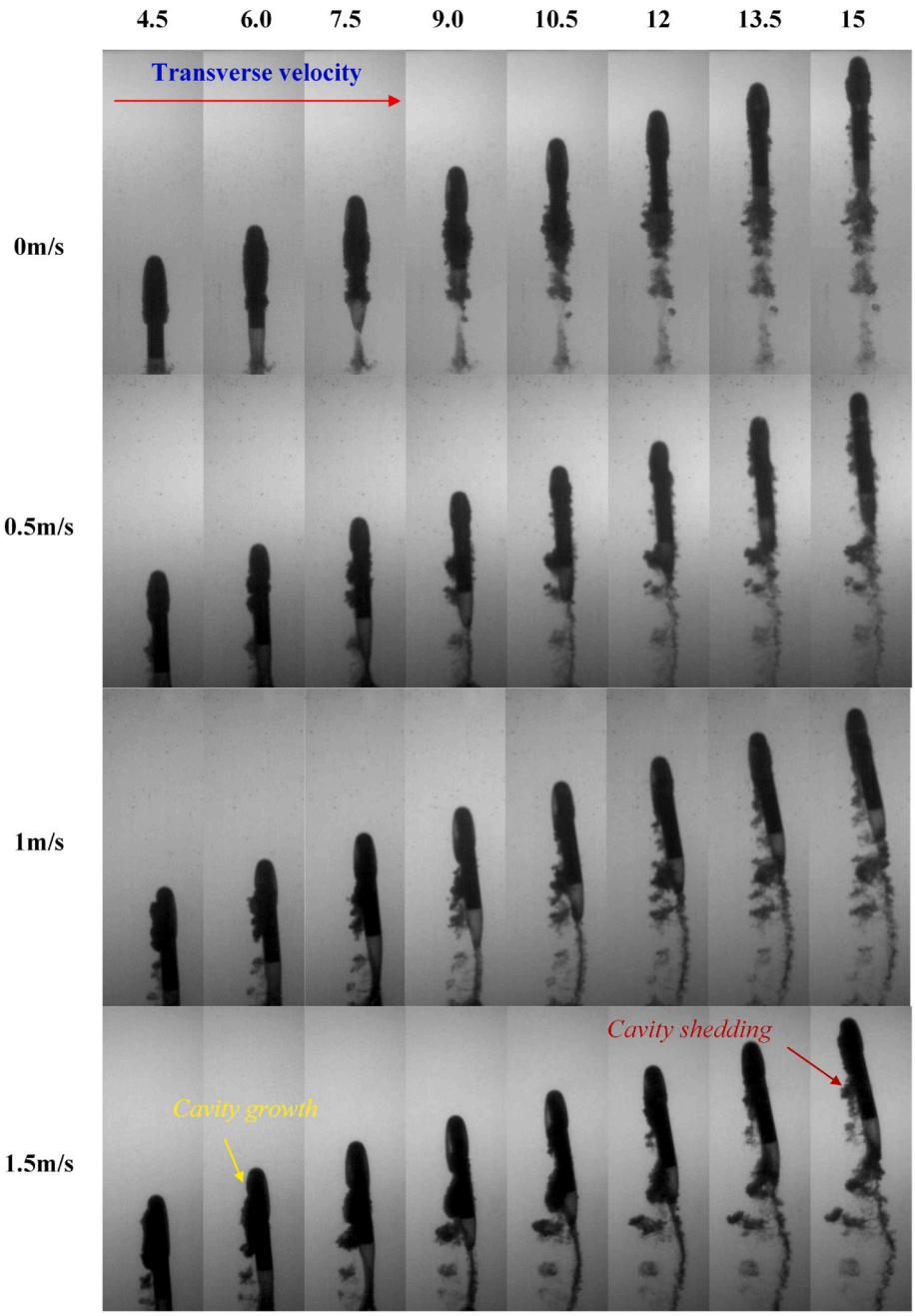


Fig. 14. Comparison of cavitation during the water traveling stage.

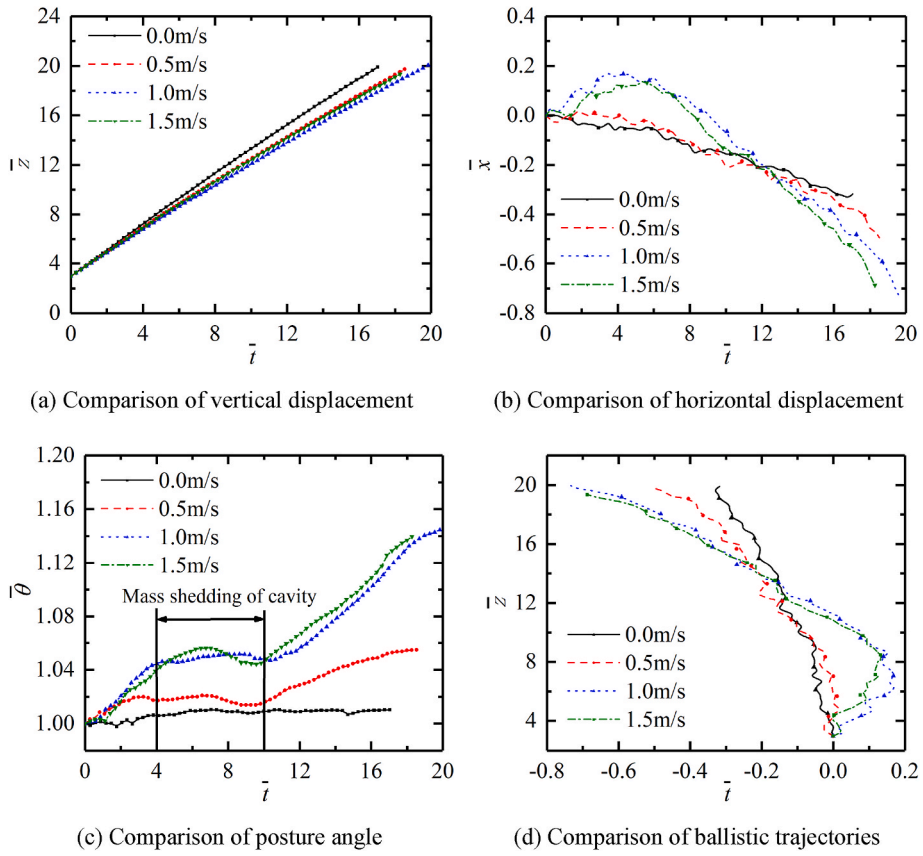
decrease in cavity thickness and appear the re-entry jet at the tail closure of the cavity (t = 0 ms).

The development of the vehicle shoulder cavity is similar in the remaining tests, however, there is a difference in the gas volume of the remaining tube outlet. According to Fig. 12, the remaining volume of the tube outlet decreases continuously as the transverse velocity increases. Since the tube outlet constitutes the majority of the gas in the cavity, its volume also rises as the transverse velocity does. Furthermore, the cavities show remarkable asymmetry in all experiments and the cavity becomes stronger as the transverse velocity increases.

Fig. 13 depicts the time-dependent variation of cavity length and maximum thickness at the backflow side during the tube exit phase. The fracture and shedding of the cavity tail are primarily responsible for the fluctuating variation in cavity length on the back flow side. The overall length of the cavity is expanding as a result of the vehicle being continuously accelerated by the high-pressure gas in the wake as it exits the tube. It can be observed that the length of the cavity on the shoulder of the backflow side and the thickness of the cavity increase as the transverse velocity increases.

In the tube exit stage, the vehicle attitude is always in the vertical state due to the restraining effect of the launched tube wall. Then, the rear of the vehicle leaves the tube mouth, and at this moment the vertical velocity of the vehicle reaches the highest, while the horizontal velocity is just equal to the cross-flow velocity. Therefore, with its combined velocity direction and the direction of the vehicle axis, there is an angle, that is, the angle attack of the vehicle. Since the vehicle is in six degrees of freedom motion during the water-traveling stage, the attitude will be deflected under the influence of the attack angle, which affects the evolution process of its shoulder asymmetric cavity. The experimental images are given in Fig. 14 with different transverse velocities (0.0 m/s, 0.5 m/s, 1.0 m/s, and 1.5 m/s) in the stage of water traveling.

Since the cavity was been asymmetrical at the time of tube exit



(a) Comparison of vertical displacement (b) Comparison of horizontal displacement

(c) Comparison of posture angle (d) Comparison of ballistic trajectories

Fig. 15. Motion characteristics of the vehicle.

during the transverse velocity stage, the cavity also produced asymmetrically shedding and collapse behavior during water traveling period when compared to no transverse velocity. As an illustration, in a transverse velocity (1.5 m/s) experiment, the re-entry jet first appeared at the tail of the cavity on both the onward and backward sides. Then, the re-entry jet moved to the front edge of the cavity, intersected with the external liquid, and sheared off the cavity on the backward side, causing the cavity on the backward side to exhibit a large-scale shedding phenomenon while the cavity on the onward side was continuously stretched (t = 4.5 ms). The reason for this phenomenon is that the backflow is stronger than the oncoming side. With the movement of the re-entry jet, some of the gas in the cavity is squeezed and flows to the oncoming side, increasing the size of the cavity on the oncoming side.

After the re-entry jet shears off the cavity, the shed cloud-like cavity slides down along the vehicle surface, while the backflow side begins to generate a new cavity (t = 6 ms). The gas in the oncoming cavity begins to flow back to the backflow side during the growth of the new cavity on the backflow side due to the pressure difference, which causes the length of the oncoming cavity to gradually start to shorten until a new re-entry jet is generated at the tail closure of the cavity on the backflow side (t = 9 ms). The re-entry jet is more likely to intersect with the boundary of the cavity wake because the newly grown cavity thickness is less than that of the cavity when it first emerged from the tube mouth. This causes a continuous small-scale shedding and collapse phenomenon at the cavity wake (t = 12 ms). The experiments of various speed reveals that the size of the first large-scale shearing and shedding of the backflow cavity and the scale of the newly grown shoulder cavity both increase as transverse speed increases.

4.3.2. *Effect of motion characteristics with different transverse velocities*

According to the previous description, the vehicle has an attack angle in the water traveling process, thus, its attitude and trajectory show a significant deflection during the period of the movement. The dimensionless vertical displacement, dimensionless horizontal displacement, dimensionless angular displacement, and dimensionless ballistic trajectory variation for the vehicle are all shown in Fig. 15.

It can be seen that the vertical displacement growth rate without transverse velocity is greater than that with transverse velocity. That is, under the influence of lateral velocity, a portion of the kinetic energy in the vertical direction is converted into kinetic energy in the horizontal direction and rotational kinetic energy, resulting in a smaller increase in vertical displacement at the same time. The vertical displacement growth rate decreases as the transverse velocity increases (Fig. 15(a)). Because it is difficult to ensure the absolute verticality of the launched tube during the experiment, the vehicle is subjected to an additional deflecting moment due to the uneven high pressure of the tube outlet and other influencing factors, resulting in a certain ballistic deflection phenomenon (Fig. 15(d)).

In this working condition, the horizontal speed is equal to the transverse speed when the vehicle leaves the tube mouth. At the initial moment, the centroid of the vehicle moves in the same direction as the transverse velocity. Next, the horizontal velocity attenuates to zero and then moves to the opposite velocity under the action of the asymmetric pressure difference on both sides of the vehicle. Therefore, under this condition, the horizontal displacement increases firstly, then decreases, and finally increases in the opposite direction (Fig. 15(b)). Due to the existence of the attack angle, there is an asymmetric pressure on both sides of the vehicle head, so the corresponding counterclockwise deflection moment causes the attitude angle to increase continuously. And the higher the transverse speed, the greater the increase in the attitude angle. From Fig. 15(c), it can be found that under the influence of transverse speed, the vehicle attitude angle increases, then decreases, and finally increases rapidly, and the attitude angle decreases within a dimensionless period. This period is just falling off from the shoulder to

the separation of the rear of the vehicle in the process of the cavity on the downstream side, which can be found by observing the images at the corresponding time. It can be seen when the cavity on the downstream side falls off on a large scale, the shed cloud-like air mass moves toward the rear along the surface of the vehicle, resulting in a corresponding low-pressure area at the tail on the downstream side. The vehicle is subjected to a clockwise moment, which offsets the effect of the counterclockwise deflection moment of the head, causes the attitude angle to deflect clockwise so that the attitude angle presents a downward trend under the influence of this low-pressure area. Finally, the shed cloud-like air mass is separated from the rear of the vehicle, the rear pressure on the leeward side increases, and its attitude angle rises again, which is affected by the deflection moment on the head.

5. Conclusions

The experimental study on underwater vertically launched vehicle was conducted in this paper based on the high-speed camera technology with different launch velocities and transverse speeds. The cavitation flow and motion characteristics were analyzed, and the main findings were as follows:

1) The initial growth of the cavity and the re-entry jet occurred in the tube-exit stage. The cavity shedding phenomena occur at different scales in the water-traveling period. During the water-exit stage, the cavities collapse, and the collapsing load impacts the vehicle wall, causing significant sputtering on its surface.
2) As the launch velocity rises, the initial cavity length will increase and the moment when the cavity separates from the gas mass at the tube mouth will be postponed. Moreover, the moment of completely shedding the cavity delays during the water exit process. Furthermore, the effect of speed on the evolution of cavitation is much greater than the effect of depth.
3) With the increase of transverse speed, the size of the initial shed cavity on the dorsal side increases, and the scale of the newly grown shoulder cavity increases accordingly. In the horizontal direction, centroid of the vehicle moves in the direction of transverse speed, and then in the opposite direction. The attitude angle shows an increasing trend in general, but its growth rate slows down in the dimensionless period $\bar{t} = 4 \sim 10$. The higher the transverse speed is, the greater the increase of attitude angle is.

Declaration of competing interest

The authors declare that they have no known competing financial interests or personal relationships that could have appeared to influence the work reported in this paper.

Acknowledgments

We are thankful to the National Natural Science Foundation of China (Grant Nos. 52171324and U21B2055) and the Fundamental Research Funds for the Central Universities (Grant No. 3102019JC006) for their financial support of our research work.

References

Ausoni, P., Farhat, M., Escaler, X., 2007. Cavitation influence on von kárm'an vortex shedding and induced hydrofoil vibrations. J. Fluid Eng. 129, 966–973.
Blake, J., Gibson, D., 1987. Cavitation bubbles near boundaries. Annu. Rev. Fluid Mech. 19, 99–123.
Boštjan, G., Matjaž, H., Andrej, P., 2010. Experimental and numerical analysis of the impact of particles on the development of cavitation flow around a hydrofoil. J. Energy Resour. Technol 3 (4), 47–63.
Callenaere, M., Franc, J.P., Michel, J.M., Riondet, M., 2001. The cavitation instability induced by the development of a re-entrant jet. J. Fluid Mech. 444, 223–256.
Chen, Y., Li, J., Gong, Z., Chen, X., Lu, C., 2021. LES investigation on cavitating flow structures and loads of water-exiting submerged vehicles using a uniform filter of octree-based grids. Ocean Eng. 225, 108811.
Franc, J.P., Michel, J.M., 2006. Fundamentals of Cavitation". Springer Science & Business Media.
Gao, S., Shi, Y., Pan, G., 2021. Numerical investigation on fluid dynamic characteristics around shoulder ventilation of submarine-launched vehicle. J. Northwest. Polytech. Univ. 39 (3), 463–470.
Gao, S., Shi, Y., Pan, G., Quan, X.B., 2022a. A study on the flow interference characteristics of projectiles successively launched underwater. Int. J. Multiphas. Flow 151, 104066.
Gao, S., Shi, Y., Pan, G., Quan, X.B., 2022b. The transient vortex structure in the wake of an axial-symmetric projectile launched underwater. Phys. Fluids 34 (6).
Hu, J., Zhang, W., Wang, C., Sun, S., Gou, C., 2021. Impact of skew on propeller tip vortex cavitation. Ocean Eng. 220, 108479.
Huang, H.B., Long, Y., Ji, B., 2020. Experimental investigation of vortex generator influences on propeller cavitation and hull pressure fluctuations. J. Hydrodyn. 32 (6).
Jin, D.Q., Wang, C., Cao, W., et al., 2011. Numerical simulation and experimental study of ventilated supercavity of underwater vehicle. Acta Armamentarii 32 (10), 1184–1188.
Kawakami, E., Arndt, R., 2010. Investigation of the Behavior of Ventilated Supercavities" 57, vol. 64.
Leroux, J.B., Astolfi, J.A., Billard, J.Y., 2004. An experimental study of unsteady partial cavitation. Fluids Eng 126, 94–101.
Li, X.Y., Ji, Y.G., Liu, X.L., Xue, S., 2019. Numerical study on cavitation characteristics of high speed fuel centrifugal pump. IOP Conf. Ser. Mater. Sci. Eng. 688 (2).
Louf, J.F., Chang, B., Eshraghi, J., Mituniewicz, A., Vlaachos, P.P., Jung, S., 2018. Cavity ripple dynamics after pinch-off. J. Fluid Mech. 850, 611–623.
Lu, J.X., Wang, C., Wei, Y.J., Sun, T.Z., Liu, F., Xu, H., 2022a. Experimental and theoretical investigation of the cavity dynamics of underwater launched vehicles. Ocean Eng. 254, 111291.
Lu, J.X., Bi, D., Wang, C., et al., 2022b. Research on the interference characteristics of successively launched underwater vehicles. Phys. Fluids 34 (6), 067117.
Marian, B., Milada, K., Jana, J., 2020. Cavitation Flow of Oil and Water through the Nozzle", vol. 328. MATEC Web of Conferences.
Pant, C.S., Frankel, S.H., 2021. Interaction between surface blowing and re-entrant jet in active control of hydrofoil cavitation. Ocean Eng. 242.
Quan, X.B., Li, Y., Wei, H.P., et al., 2008. Cavitation collapse characteristic research in the out-of-water progress of underwater vehicles. J. Ship Mech. 12(004), 545–549.
Ramirez, R., Avila, E., Lopez A Bula, L., Forero, J.D., 2020. CFD characterization and optimization of the cavitation phenomenon in dredging centrifugal pumps. AEJ - Alexandria Engineering Journal 59 (1).
Shao, S., Wu, Y., Haynes, J., Rea, Arndt, Hong, J., 2018. Investigation into the behaviors of ventilated supercavities in unsteady flow. Phys. Fluids 30 (5), 052102.
Shi, Y., Ren, J., Gao, S., et al., 2021. Numerical investigation on air film fusion of pressure-equalizing exhaust around shoulder ventilation of submarine-launched vehicle. J. Mar. Sci. Eng. 10 (1), 39.
Sun, T., Xie, Q., Li, X., Zou, L., 2021a. Numerical investigation of the effects of free surface on tip-leakage vortex cavitation behaviors over a NACA0009 hydrofoil. Int. J. Multiphas. Flow 141 (4), 103671.
Sun, T.Z., Zhang, X.S., Zhang, J.Y., Wang, C., 2021b. Experimental study on the unsteady natural cloud cavities: influence of cavitation number on cavity evolution and pressure pulsations. J. Mar. Sci. Eng. 9 (5), 487.
Sun, T.Z., Xie, Q., Huang, H., et al., 2022. Numerical investigation of ventilated vacuole dynamics over a submerged body in the wake of a propeller. Ocean Eng. 257, 111580.
Tan, Z.K., Zhang, M.D., Huang, G.H., Huang, B., 2022. Collapsing behavior of a spark-induced cavitation bubble near the air bubble attached to the tube nozzle. Ocean Eng. 253, 111183.
Wang, Y.W., Huang, C.G., Wu, X.C., Du, T.Z., Yu, X.X., 2015. Investigation of cavities shedding condition on underwater vehicles in the vertical launch process. Eng. Mech. 32 (11), 33–39.
Wang, Y., Wu, X., Huang, C., et al., 2016. Unsteady characteristics of cloud cavitating flow near the free surface around an axisymmetric vehicle. Int. J. Multiphas. Flow 48–56.
Wang, X., Han, Z.Q., Su, W.H., 2017. Numerical study of the impact on high-pressure and evaporating spray behavior of nozzle cavitation at typical diesel engine conditions. Int. Commun. Heat Mass Tran. 81.
Wang, Y.W., Huang, C.G., et al., 2016. On the Internal Collapse Phenomenon at the Closure of Cavitation Bubbles in a Deceleration Process of Underwater Vertical Launching. Applied Ocean Research 56, 157–165.
Xu, W.H., He, X.K., Xiao, H., Wang, W., 2021. Influence of wall roughness on cavitation performance of centrifugal pump. J. Braz. Soc. Mech. Sci. Eng. 43 (6).
Yin, R., Liu, H., He, Z.Y., 2022. Numerical simulation of hydrofoil cavitation. J. Phys. Conf. 2206 (1).
Yu, X., Wang, Y., Huang, C., et al., 2015. Experiment and Simulation on Air Layer Drag Reduction of High-Speed Underwater Axisymmetric Vehicle. Eur. J. Mech. B Fluid 52, 45–54.
Zhang, X., Wang, C., Wei, Y., et al., 2016. Experimental investigation of unsteady characteristics of ventilated cavitation flow around an under-water vehicle". Adv. Mech. Eng. 8 (11), 1687814016678198.
Zhao, M.S., Zhao, W.W., Wan, D.C., 2020. Numerical simulations of propeller cavitation flows based on OpenFOAM. J. Hydrodyn. 32 (4).